Geophysical Journal International

Geophys. J. Int. (2009) **179,** 1817–1830 doi: 10.1111/j.1365-246X.2009.04385.x

Depth extent of damage zones around the central Calaveras fault from waveform analysis of repeating earthquakes

Peng Zhao and Zhigang Peng

School of Earth and Atmospheric Sciences, Georgia Institute of Technology, Atlanta, GA 30332*, USA. E-mail: pzhao@gatech.edu*

Accepted 2009 September 14. Received 2009 September 12; in original form 2009 June 21

SUMMARY

We systematically investigate spatial variations of temporal changes and depth extent of damage zones along the Calaveras fault that ruptured during the 1984 Morgan Hill earthquake by the waveform analysis of 333 sets of repeating earthquakes. We use a sliding window waveform cross-correlation technique to measure traveltime changes in waveforms generated by each repeating cluster. We find clear traveltime delays in the *S*- and early *S*-coda waves for events immediately after the Morgan Hill main shock. The amplitudes of the time delays decrease logarithmically with time since the main shock, indicating a time-dependent recovery (healing) process following the abrupt coseismic temporal changes. The largest temporal changes are observed at station CCO that is the closest to the rupture zone of the Morgan Hill main shock. The time delays at this station are larger for clusters in the top 6 km, and decrease systematically at larger depth. In comparison, the time delays observed at other five stations are much smaller, and do not show clear relationship with hypocentral depth. We suggest that the temporal changes at these five stations mostly occur in the top few hundred metres of the near-surface layers, while the temporal changes at station CCO are likely associated with the damage zone around the Calaveras fault that is well developed in the top few kilometres of the upper crust. Our results are consistent with the inference of a widespread damage and non-linearity in the near-surface layers associated with strong ground motions of nearby large earthquakes, and localized damages and flower-type structures around active faults based on previous studies of fault zone structures and recent 3-D numerical simulations.

Key words: Fault zone rheology, Earthquake ground motions; Site effects; Wave propagation; Fractures and faults.

GJI Seismology

1 INTRODUCTION

Measuring temporal changes around active fault zones (FZs) has been a long-sought goal in seismological community for many decades. A better understanding of the temporal evolution of FZ properties during earthquake cycles has important implications for many aspects of earthquake physics, including long-term evolutions of FZ structures, interaction of earthquakes and faults and seismic hazard mitigation. In the last 20 yr, many studies have succeeded in documenting temporal changes in the upper crust associated with the occurrences of large earthquakes based on waveform analysis of microearthquakes (Poupinet *et al.* 1984; Rubinstein & Beroza 2004a,b, 2005; Schaff & Beroza 2004; Li *et al.* 2006; Peng & Ben-Zion 2006; Rubinstein *et al*. 2007; Taira *et al.* 2008, 2009), repeatable controlled sources (Vidale & Li 2003; Nishimura *et al.* 2005; Li *et al.* 2006), spectral ratio methods (Sawazaki *et al.* 2006, 2009; Karabulut & Bouchon 2007; Wu *et al.* 2009a,b), and seismic interferometry (Wegler & Sens-Schönfelder 2007; Brenguier *et al.* 2008a,b; Ohmi *et al.* 2008; Sleep 2009; Wegler *et al.* 2009; Xu & Song 2009). Their results generally show clear reduction of seismic velocities (Schaff & Beroza 2004; Rubinstein & Beroza 2004a,b, 2005; Peng & Ben-Zion 2006; Rubinstein *et al*. 2007), waveform coherencies (Baisch & Bokelmann 2001), or increase of attenuation (Chun *et al.* 2004) during strong ground motions of nearby large earthquakes. The observed temporal changes are most likely caused by widespread damages in the near surface layer and around active FZs associated with the strong ground motion and/or dynamic ruptures of nearby large earthquakes (e.g. Rubinstein & Beroza 2004a; Li *et al.* 2006; Peng & Ben-Zion 2006; Ma 2008; Chao & Peng 2009). The observed coseismic temporal changes, typically on the order of a few percent or less, are generally followed by logarithmic recoveries on the time scales of several months to years, indicating healing or restrengthening processes of the damaged FZ rocks or near-surface layers (e.g. Vidale & Li 2003; Rubinstein & Beroza 2004a,b; Peng & Ben-Zion 2006).

One of the outstanding questions in studying temporal changes in the upper crust is the depth extent of the damage zone. Here we use the term ‘damage zone’ to represent the layer that has experienced significant fracturing or other types of damages in material strength during large earthquakes, resulting in clear temporal changes in seismic properties. A related term is ‘fault zone’, which represent highly fractured low-velocity layers surrounding a fault

interface (e.g. Ben-Zion & Sammis 2003). As mentioned above and will be discussed further below, both active FZs and near-surface layers are two likely candidates of damage zones formed due to the occurrence of nearby large earthquakes (e.g. Ma 2008). Indeed, recent studies based on repeating earthquakes (Rubinstein & Beroza 2005; Peng & Ben-Zion 2006) and seismic interferometry (Sleep 2009) have shown that the coseismic velocity reduction is mostly confined in the top 100–200 m of the near-surface layers. This observation is generally consistent with the laboratory observations and numerical simulations that non-linear elasticity decreases with increasing compressive stress (i.e. depth) (Zinszner *et al.* 1997; Johnson & Jia 2005; Ma 2008; Finzi *et al.* 2009). In comparison, other studies have shown that the coseismic temporal changes near active FZs could occur at much greater depth in the seismogenic zone (Schaff & Beroza 2004; Li *et al.* 2006; Rubinstein *et al.* 2007) or near the brittle–ductile transition zone (Taira *et al.* 2008). Hence, it is still not clear how to put these different observations together into a coherent picture of temporal changes in the upper crust associated with the occurrence of nearby large earthquakes.

Recently, Ma (2008) presented a unifying interpretation of both observations by simulating 3-D dynamic rupture propagation on a vertical strike-slip FZ based on a pressure-dependent yield criterion in the upper crust. Because the yield stress depends on the confining pressure, the yielding occurs more easily near the surface than at depth. His simulation produces widespread inelastic zones away from the active FZ with a thickness of a few hundred metres or less, and a flower-type structure around active faults with broad inelastic zone in the top few kilometres of the crust and highly localized inelastic strain at depth. This explains both the near-surface damage and FZ damage at depth as observed in previous studies. A similar flower-type structure is obtained by Finzi *et al.* (2009), who performed 3-D numerical simulations in a seismogenic upper crust governed by a continuum brittle damage framework. These numerical simulations suggest that the damages in the near surfaces and within FZ at depth could be observable through seismic observations, and likely exist in both the regions.

Reliable detection of temporal changes generally requires collocated seismic sources (i.e. repeating earthquakes or artificial sources), so that the observed changes in traveltimes or waveform coherencies are mainly attributed to temporal changes in the medium, rather than spatial variations in the seismic sources (e.g. Peng & Ben-Zion 2005, 2006). In addition, many repeating sources at different depths are needed to better constrain the spatial variations and depth extent of the damage zone. In this study, we use more than 300 repeating clusters occurred along the central Calaveras fault in northern California to study temporal changes and depth extent of the damage zone associated with the occurrence of the 1984 M_L6.2 Morgan Hill earthquake. The repeating earthquakes occurred at the depth range of 1–10 km, and the corresponding waveforms are recorded by stations at variable distances from the rupture zone, allowing us to place a tight constraint on the spatial and depth extent of the damage zone.

Schaff & Beroza (2004) have used repeating earthquakes from this region to quantify temporal changes associated with the 1984 Morgan Hill earthquake. Our study is largely motivated by their success, but differs from that of Schaff & Beroza (2004) in the following aspects. First, Schaff & Beroza (2004) examined a wide region surrounding the rupture zones of the 1984 Morgan Hill earthquake and the 1989 Loma Prieta earthquakes based on waveforms generated by about 20 repeating clusters. In comparison, we focus on the immediate vicinity of the fault segment that ruptured during the 1984 Morgan Hill earthquake and used more than 300 repeating clusters to provide a better constraint on the spatial and depth extent of the damage zone. In addition, we use slightly different techniques to compute the time delays and quantify temporal changes. As will be shown below, our results are largely compatible with those from Schaff & Beroza (2004) and other recent studies (Rubenstein & Beroza 2004a,b; Rubinstein *et al.* 2007; Li *et al.* 2006; Peng & Ben-Zion 2006), and confirm the aforementioned 3-D numerical simulations on near-surface and FZ inelastic strains and the depth extent of the inelastic zone (Ma 2008; Finzi *et al.* 2009). In the next section, we first describe the steps to identify repeating earthquakes in our study region. In Section 3, we provide the detailed analysis procedure to measure temporal changes from waveforms of repeating earthquakes. The results are shown in Section 4 and discussed in Section 5.

2 BACKGROUND AND REPEATING CLUSTER IDENTIFICATION

The Calaveras fault is one of the most active branches of the San Andreas Fault (SAF) system in northern California. It has generated at least 14 earthquakes with $M > 5$ since 1850 (Oppenheimer *et al.* 1990; Manaker *et al.* 2005), with the most recent M_w 5.6 event near Alum Rock on 2007 October 31. The largest event was the M_L 6.2 1984 April 24 Morgan Hill earthquake that ruptured the central portion of the Calaveras fault (Bakun *et al.* 1984; Fig. 1). Numerous aftershocks of the Morgan Hill main shock were well recorded by the Northern California Seismic Network (NCSN) since then.

Using waveform cross-correlation and a double-difference method (Waldhauser & Ellsworth 2000), Schaff *et al.* (2002) relocated the seismicity along the central Calaveras fault around the rupture zone of the 1984 Morgan Hill earthquake. They found that earthquakes in this region are highly clustered in space and form repeating clusters. Using this relocated catalogue, Zhao & Peng (2008) identified 353 sets of repeating clusters (with at least five events in each cluster) around the rupture zone of the 1984 Morgan Hill earthquake. Their identification procedure was solely based on the magnitude difference and overlapping rupture areas, and did not take into account waveform similarities. To further improve the quality of the obtained repeating clusters, we add another constraint based on waveform similarities, which has been proven to be effective in discriminating repeating clusters at short interevent distances (e.g. Nadeau *et al.* 1995; Menke 1999; Schaff *et al.* 2002; Templeton *et al.* 2008, 2009).

Our criteria of identification of repeating clusters generally follow those of previous studies (e.g. Nadeau *et al.* 1995; Waldhauser & Ellsworth 2002; Waldhauser & Schaff 2008; Lengliné & Marsan 2009). We require that each event pair within the same cluster has a magnitude difference of less than 1, 50 per cent overlapping of rupture areas with the assumption of a circular crack model (Eshelby 1957) and a nominal 3-MPa stress drop, and minimum median waveform cross-correlation coefficients of 0.9. The first two criteria are the same as used in Zhao & Peng (2008). To calculate the similarity of every event-pair, we use vertical-component seismograms (100 samples per second) for all events listed in Schaff *et al.* (2002) and recorded by the short-period stations in the NCSN. A 1–20 Hz band-pass filter is applied to all the data. For each station, we only use events with hypocentre distances less than 50 km and the signal-to-noise ratio (SNR) larger than 5. Next, we compute the waveform correlation coefficients (CCs) within a 3-s time window between all possible event-pairs. The 3-s time window starts 1 s

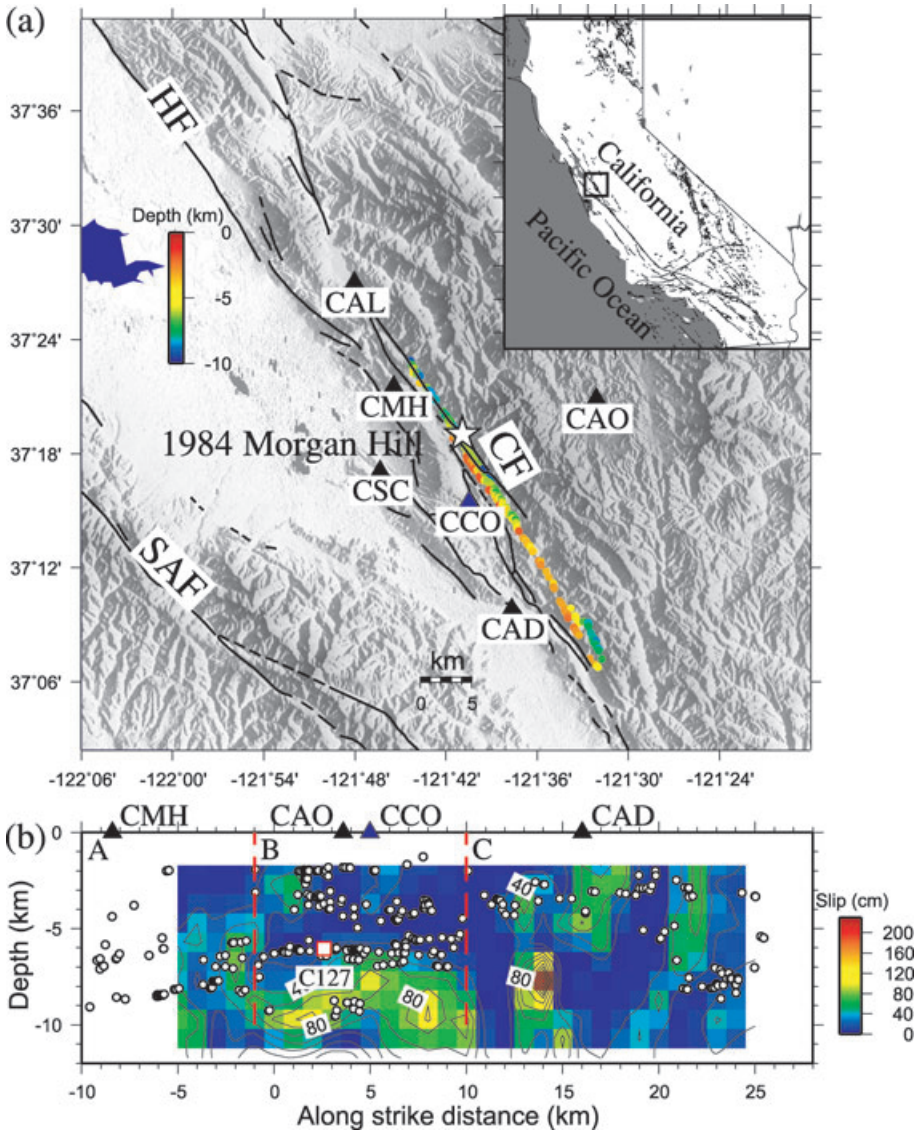

Figure 1. (a) Location of the central section of the Calaveras fault in northern California. Dark lines denote nearby faults. The circles denote the 333 repeating clusters identified in this study with color denoting their depths. The star and solid triangles mark the epicentral location of the 1984 Morgan Hill main shock and six stations used in this study, respectively. Shaded background indicates topography with white being low and dark being high. The inset shows the map of California with the box corresponding to the study area. SAF, San Andreas fault; CF, Calaveras fault and HF, Hayward fault. (b) The centroid locations of 333 repeating clusters in the cross-section map along the Calaveras fault with the strike of 146°. The background color denotes the slip distribution of the Morgan Hill main shock (Beroza & Spudich 1988). Waveforms generated by events in cluster C127 (the sold white square) are shown in Fig. 4. The seismicity are separated into three segments (A–C) divided by red dashed lines to investigate the spatial pattern of temporal changes observed at station CCO, which are shown in Figs 7 and 8.

before the predicted direct *P* arrival using a 1-D velocity model in central and northern California (Waldhauser *et al.* 2004). We then compute the median value of CCs between two events with at least three recording stations, and use it as a measure of similarity for these two events. Within each repeating cluster, we drop any event if the median value of similarities between this event and the rest is less than 0.9. After the preceding procedure, we identify a total of 333 repeating clusters (∼2650 events) with at least five events in each cluster. The relative locations and waveforms for all clusters are visually inspected to ensure the colocation of each cluster (Figs 2 and 4a).

The locations of the repeating clusters obtained from this study are largely consistent with those from previous studies (Rubin 2002; Peng *et al.* 2005) with partially overlapping regions (Fig. 3). The locations are slightly different as compared with those from another recent study in the same region (Templeton *et al.* 2009). The primary reason is that Templeton *et al.* (2009) identified repeating clusters based solely on waveform similarities without earthquake relocations. Hence, the disagreement mainly reflects the intrinsic difference between earthquake locations from the standard NCSN and relocated catalogues. A detailed comparison of these different repeating clusters is beyond the scope of this paper.

3 ANALYSIS PROCEDURE

We measure time delays for 6 stations around the rupture zone of the 1984 Morgan Hill main shock (Fig. 1a). The analysis procedure

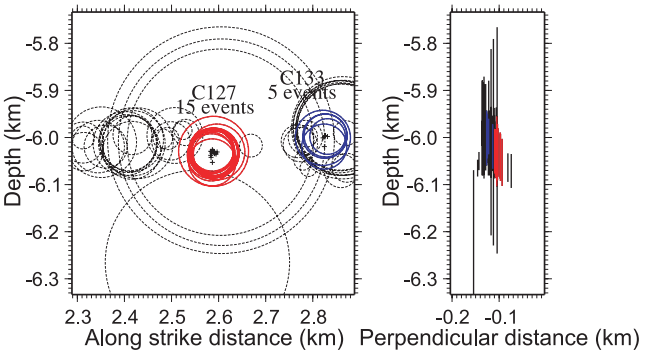

Figure 2. Cross-section views of 15 events within cluster C127 and its nearby cluster C133 (with five events) marked by the red and blue circles, respectively, from the (a) along-strike direction and (b) normal direction to the strike of the Calaveras fault. The source radius of each event is estimated from its catalogue magnitude, based on a moment-magnitude relationship, with a circular crack model (Eshelby 1957) assuming a 3-MPa stress drop.

generally follows that of Niu *et al.* (2003) and Peng & Ben-Zion (2006). First, we remove the mean values and trends and apply a bandpass filter at 1–20 Hz to all traces. Next, we select seismograms with a minimum SNR of 5, and choose a reference trace for each station–cluster pair. Since most clusters do not have events before the main shock, the waveform corresponding to the last event in each station–cluster pair is chosen to be the reference trace. Many previous studies have observed a logarithmic recovery of the coseismic damage to the pre-main shock level (Vidale & Li 2003; Peng & Ben-Zion 2006; Sawazaki *et al.* 2006, 2009), indicating that the post-seismic recovery mostly occurs within the first few months. Hence, we use the reference trace as a proxy for the pre-main shock level, assuming that the coseismic changes have fully recovered to the pre-main shock level over ∼10 yr. It is worth pointing out that such assumption is not valid if rocks have experienced permanent damages that cannot be completely recovered to the post-seismic stage (e.g. Schaff & Beroza 2004). In this case, using the last event as the reference would result in lower coseismic changes than those by using the event before the main shock as the reference.

We note that the locations of stations CAD and CCO have been changed by about 14 m at 1992 December and 130 m at 1996 April, respectively (http://www.ncedc.org/ftp/pub/doc/ncsn/ncsn.stations). After carefully checking the results from these two stations, we find that temporal changes estimated from CCO could be contaminated due to such change in the station location. Thus, for this station, we only analyse seismic data recorded prior to 1996 April. Finally, we align all other traces to the reference trace by cross-correlating a 1-s time window that is 0.2 s before the corresponding picked *P* arrivals. We also require that all other traces have a minimum CC of 0.8 with the reference trace.

After the above pre-processing steps for each station–cluster pair, a sliding window waveform cross-correlation technique (Niu *et al.* 2003; Peng & Ben-Zion 2006) is used to measure traveltime differences τ(t) and de-correlation index $D(t)$ (defined as one minus the maximum cross-CC between two events) of subsequent traces to the reference trace in each station–cluster pair (Fig. 4). The time window is 1-s long, sliding 2 s before and 15 s after aligned *P* arrivals, with sliding interval of 0.1 s in each step. A cosine taper is applied to each time-window with 10 per cent of the entire width to reduce the Gibbs' phenomenon (Niu *et al.* 2003; Peng & Ben-Zion 2006). To increase the precision of measured time delays, we linearly interpolate the bandpass-filtered vertical seismograms from 100 to 10 000 s^{-1} before calculating the traveltime differences and de-correlation indexes. Fig. 4 shows an example from Cluster 127 recorded at station CCO. The measured traveltime differences are mostly positive, corresponding to reductions in seismic velocities, and the overall amplitudes of time delays decrease with time since the main shock (Fig. 4). The decorrelation indexes also show similar patterns after the main shock. In this study, we only use traveltime differences to quantify the temporal variations of seismic velocity in the study region.

For each station–cluster pair, we use the median value of the calculated time delays within a 6-s time window to qualify the traveltime changes relative to the reference trace. We do not fit the slope of the measured time delays, as was done in some previous studies (e.g. Poupinet *et al.* 1984; Schaff & Beroza 2004; Rubinstein *et al.* 2007), because we find that in most cases time delay does not increase monotonically with the traveltime (e.g. Fig. 4b). In addition, our synthetic tests in Appendix A have shown that the median value could be used as a better parameter to quantify the depth dependence of temporal changes than the slope. We compute the median, instead of the mean value to avoid potential contaminations from glitches in the traveltime delays (mostly due to low SNR). The 6-s time window is 0.1 s before the manually picked direct *S* arrival (Fig. 4), so that it contains both direct *S* and early *S* coda waves. Including early *S* coda wave helps to stabilize our results at each station, because of the averaging effect due to superposition of scattered waves from all the possible azimuths and paths (Aki 1969). In addition, the traveltime differences in the early *S*-coda waves are generally much larger than those in the direct *S* waves (e.g. Rubinstein *et al.* 2004a; Schaff & Beroza 2004; Peng & Ben-Zion 2006), allowing us to better quantify the difference in each event-station pair. We do not include the late *S*-coda waves mainly because of the diminishing SNR with increasing traveltime. We note that the time delays calculated in this study reflect the changes of the

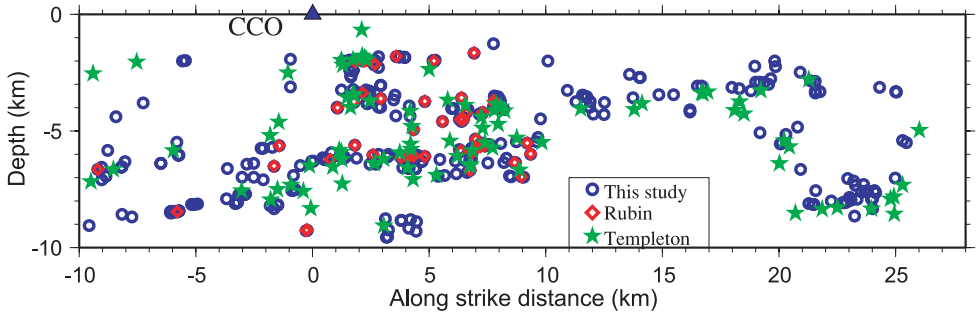

Figure 3. Comparison of centroid locations of repeating clusters from our study (blue open circles), Rubin (2002) (red open diamonds) and Templeton *et al.* (2009) (green asterisks) in the cross-section view along the Calaveras fault.

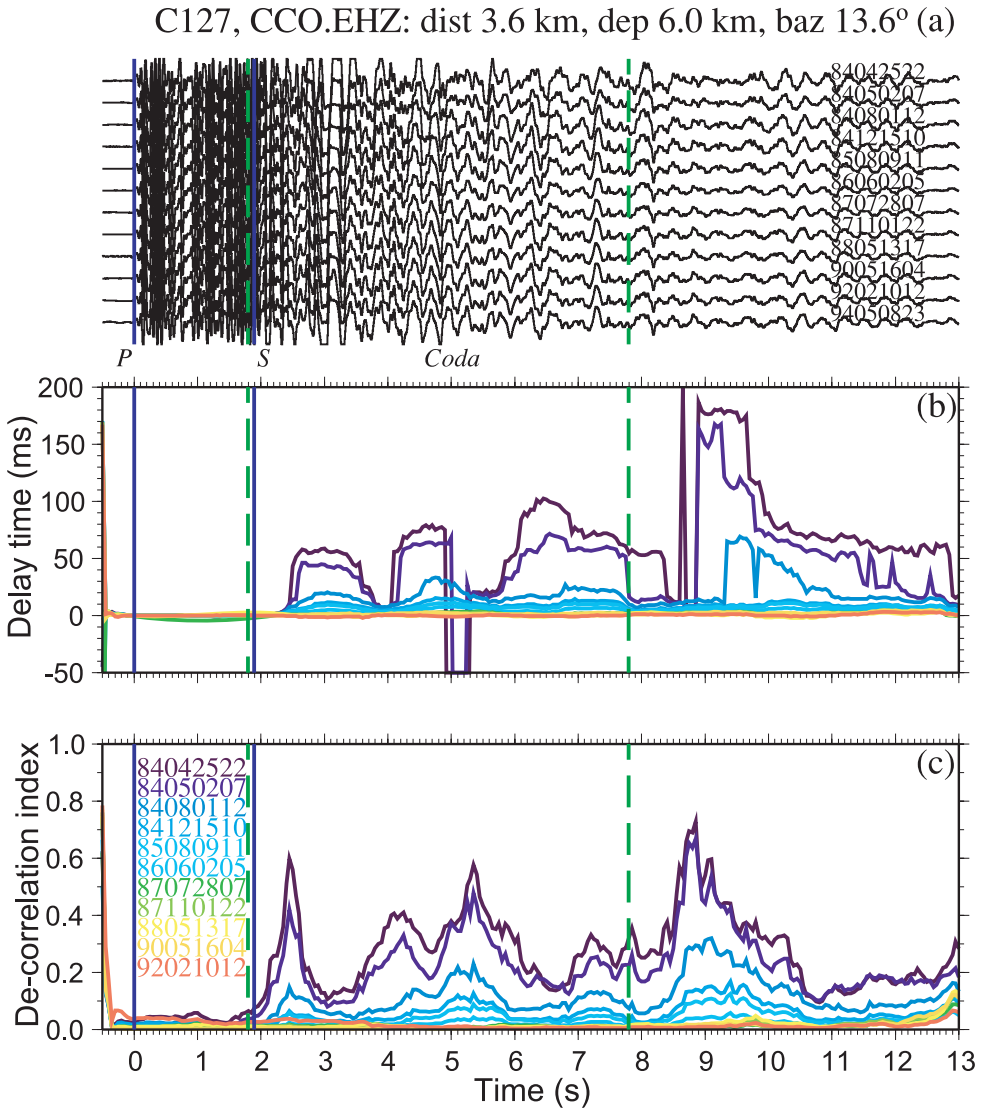

Figure 4. (a) Vertical-component seismograms generated by the 15 events in cluster C127 and recorded by station CCO. Seismograms are aligned by *P* waves at 0 s. Calculated (b) delay time τ(t) and (c) decorrelation index. The green vertical dashed lines denote the 6-s time window with 0.1 s before direct *S* waves, which is used to compute the median delay time. The event ID members are marked on the panels (a) and (c), consisting of the occurrence time of corresponding event (2-digit-year, 2-digit-month, 2-digit-day and 2-digit-hour).

differential arrival times between *S* and *P* waves, because of the alignment of *P* arrivals in the previous steps. In reality, several studies have observed temporal changes in the *P* waves, although the values are much smaller than for the *S* waves (Schaff & Beroza 2004; Li *et al.* 2006). Hence, the obtained temporal changes are probably lower bounds (Rubinstein & Beroza 2004a; Peng & Ben-Zion 2006).

Fig. 5 shows the median time delay of each event versus the lapse time since the main shock for the six stations. The median time delays generally follow a linear decay trend with the logarithmic lapse time, consistent with previous studies (e.g. Peng & Ben-Zion 2006). Therefore, we linearly fit the trend with a least-squares method for each station and calculate the slope of the post-seismic recovery (Fig. 5). We also find clear increase of time delays at most stations on 1986 March 31, which corresponds to the occurrence time of an M_L5.7 event near Mt Lewis in this region (Zhou *et al.* 1993). This event is the largest earthquake occurred within 50 km after the 1984 Morgan Hill earthquake. To avoid potential contaminations in the time delays from this event, we only fit the data before its occurrence time (Fig. 5).

4 SPATIAL VARIATIONS OF TEMPORAL CHANGES

4.1 General observations

Because most clusters do not have events before the Morgan Hill main shock, we use the slope of least-squares fitting and time delays at 24 hr (1 d) after the main shock (i.e. computed from the slope and intercept at one day of the least-squares fitting) as a proxy for the coseismic changes. Although the temporal changes are much larger during and immediately after the main shock (e.g. Sawazaki *et al.* 2006, 2009; Wu *et al.* 2009a,b), we do not have enough repeating events within this period, especially at larger depth, to provide a better constraint. As shown in Fig. 5, all six stations have

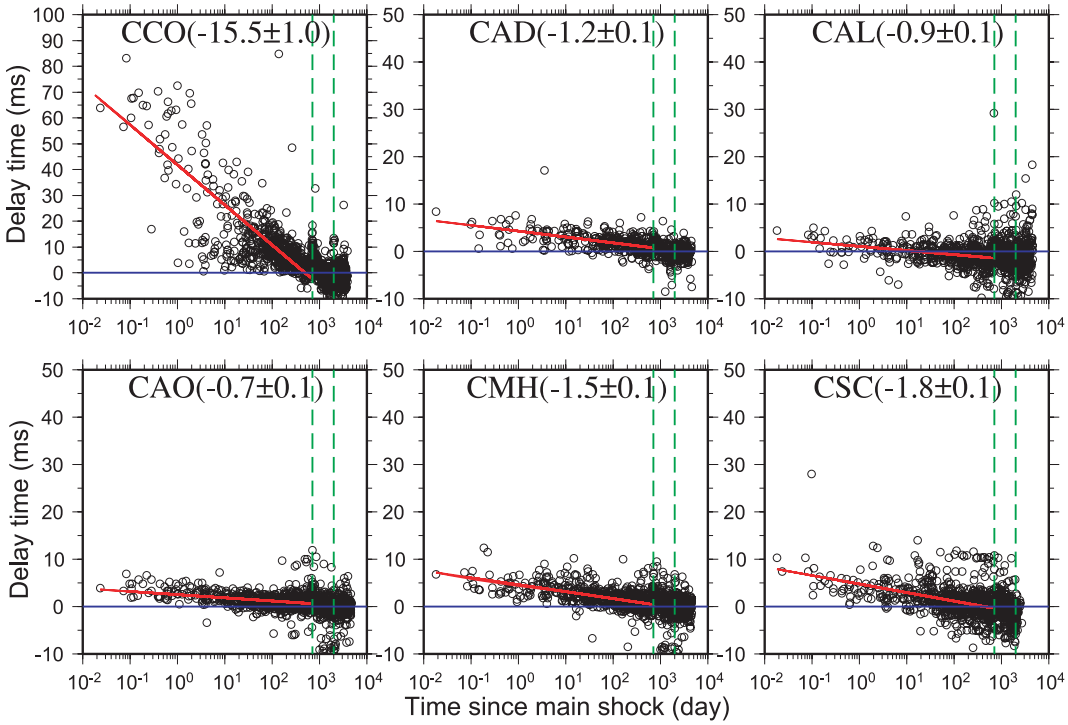

Figure 5. Median delay time plotted against the logarithmic elapsed time since the 1984 Morgan Hill earthquake for the vertical-component seismograms recorded at the six stations. The red line in each panel represents a least-squares fit to the data. Two green dashed vertical lines mark the occurrence times of a local 1986 M_L5.7 event and the 1989 Loma Prieta earthquake, respectively. In this study, we only fit the data before the 1986 event. The station name is labeled in the top part of each panel, with the slope (in the unit of ms per decade) and the standard deviation of the least-squares fitting.

positive coseismic temporal changes, corresponding to reductions of seismic velocities in this region. However, their amplitudes are quite different. The largest temporal change is shown at station CCO, with a slope of approximately −15 ms per decade change in time and time delay of ∼40–70 ms at one day after the main shock. In comparison, the values at other five stations (i.e. CAL, CSC, CMH, CAO, and CAD) are much smaller, with slopes of approximately −1 ms per decade and time delays of less than 10 ms. Fig. 5 also shows that the time delays at the five stations generally follow the logarithmic recovery trends without significant deviation, indicating a weak dependence of time delays on the locations of repeating clusters. In comparison, the time delay measurement at station CCO is more scattered than that for other five stations.

To further illustrate this, we plot in Fig. 6 the time delay at 1 d after the main shock from the least-squares fitting for each repeating cluster versus its depth. We find no systematic relationship between the time delays and the hypocentral depths for those five stations. In comparison, we find that the time delays at CCO are scattered in the top 6 km, but weakly decrease from 6 to 10 km. The overall CC between the time delays and depths is 0.36. If we select only events below 6 km, the CC value is 0.51. Although both values are relatively low, we can rule out the probability of random occurrence at 95 per cent confidence level.

4.2 Possible regions of temporal changes

To better understand the physical processes corresponding to the observed temporal changes, it is important to constrain the regions where temporal changes have occurred. The temporal changes could arise from source regions, propagation paths, and in the near-surface layers beneath the station (e.g. Rubinstein & Beroza 2004a; Peng & Ben-Zion 2006; Rubinstein *et al.* 2007). If the temporal changes are mainly from the source region (i.e. immediately around the repeating clusters at seismogenic depth), we would expect the time delays calculated from different stations for the same repeating cluster to be similar. If the temporal changes are mostly accumulated along the propagation paths, the observed time delays for a given station could vary systematically depending on the locations of repeating clusters. When the ray path between the station and repeating cluster is along or cuts across a damage zone during propagation, such as an active FZ that is further damaged during the main shock, we would expect to observe large temporal changes. On the other hand, if the seismic ray does not sample the damage zone, the observed temporal change would be much smaller. Finally, if most temporal changes are accumulated in the near surface layers, the observed time delays at a given station should be similar and do not have a strong dependence on the ray paths (i.e. the locations or the depths of the repeating clusters).

As shown in Figs 5 and 6, the time delays for the five stations (CAL, CSC, CMH, CAO, and CAD) are relatively small and we find no systematic correlation between the time delays and the hypocentral depths. Hence, we infer that the time delays are mostly accumulated in the near-surface layers beneath the five stations, which is also consistent with previous studies in this region (Schaff & Beroza 2004; Rubinstein & Beroza 2004a,b). On the other hand, the time delays at CCO are much larger and show clear scatter around the fitted line (Fig. 5) and systematic variations with hypocentral depths (Fig. 6). These observations indicate that the temporal changes are not just accumulated in the near-surface layers, but also along the ray paths at larger depth. In the following

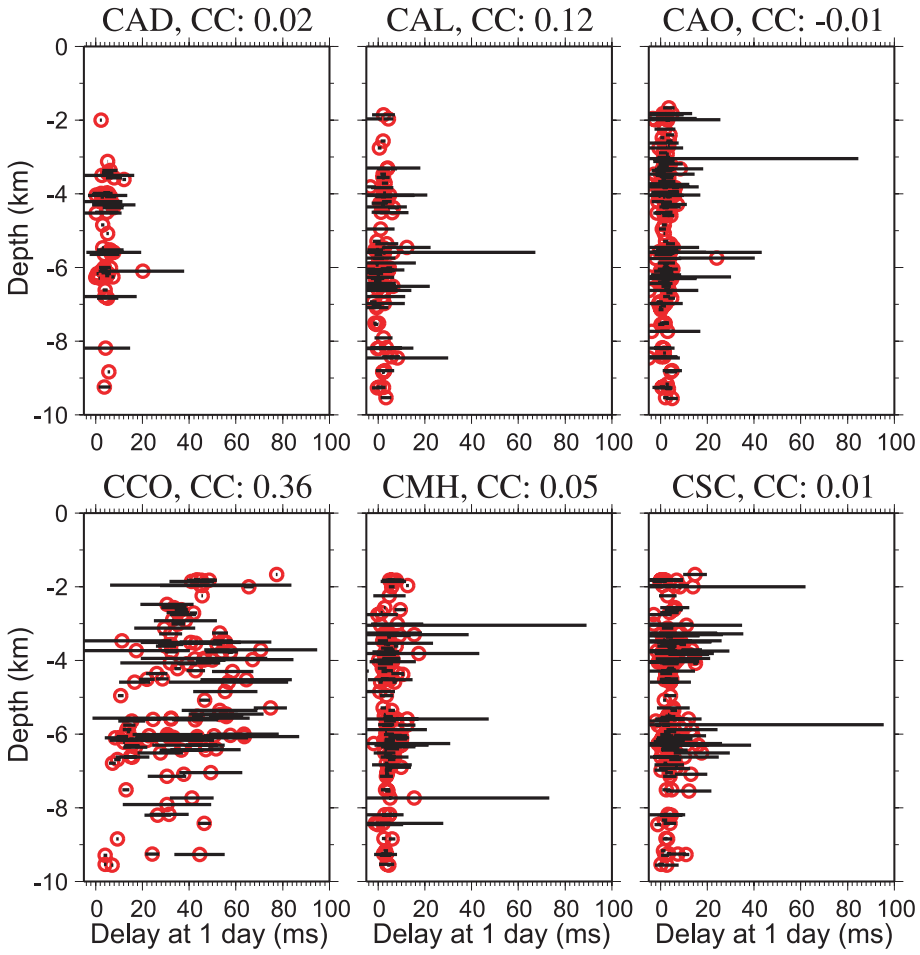

Figure 6. Delay-time at one day after the 1984 main shock versus depths of events. The delay-time is calculated from least-squares fitting for corresponding repeating cluster with at least three events occurred between the 1984 main shock and the 1986 event (see the text for details). The black horizontal lines mark the error of least-squares fitting from the corresponding events. Station name and correlation coefficient between delay-time and depths are labeled on the top of corresponding panel.

section, we focus only on the measurements at station CCO and further quantify the path and depth dependence effects.

4.3 Depth extent of the damage zone around station CCO

To verify whether time delays at CCO are path dependent, we first divide the entire repeating clusters into three segments according to their along-strike distances to CCO (Fig. 1b). We find some variations in the time delays for different segments (Fig. 7). The coseismic changes and decay rates for segments to the NW (Segment A) and SE (Segment C) sides of CCO are about the same with less scatter. The most complicated feature is from Segment B, which is directly beneath station CCO with its along-strike distance from −1 to 10 km. The decay rates in Segment B appear to follow several different trends. Similar to Fig. 6, we also plot the delay times at 1 d after the 1984 main shock for each repeating cluster at these three segments (Fig. 8). In Segment A, the clusters satisfying our criteria all occurred at the depth range of 6–9 km, and hence the delay times do not show clear variations with depth. In segment C, there is a weak increase of delay times from 2.5 to 4 km. After that, the delay times remain more or less constant. In segment B, the delay times show large variations in the top 6.5 km, and decrease significantly below 6.5 km, much clearer than the general patterns shown in Fig. 6.

Finally, we divide the Segment B into four zones based on their hypocentral depths (Fig. 9). Again we find a clear depth dependence of temporal changes. The largest coseismic change is from the shallow zone (0–5 km at depth) with a slope of −17.4 ms per decade, and the values decrease for deeper zones. In addition, the time delays for each zone generally follow a linear trend by visual inspection, except for Zone 3, which appears to have multiple distinct trends. In Zone 3, the slope of the higher decay trend is close to that of the shallow segment (i.e. Zone 1), whereas the slope of the lower decay trend is close to that of the deep segment (i.e. Zone 4).

5 DISCUSSIONS

In this study, we investigated the spatial variations and depth dependence of temporal changes along the central segment of the Calaveras fault that ruptured during the 1984 Morgan Hill earthquake. Clear temporal changes have been observed immediately after the main shock, associated with increasing arrival times in the direct *S* and early *S* coda waves. The observed time delays systematically decrease with logarithmic time since the main shock. Such time-dependent recovery is likely related to the healing processes of damaged FZ rocks or near-surface layers as inferred from many previous studies (Vidale & Li 2003; Schaff & Beroza 2004; Peng & Ben-Zion 2006). We also found clear spatial variations in the

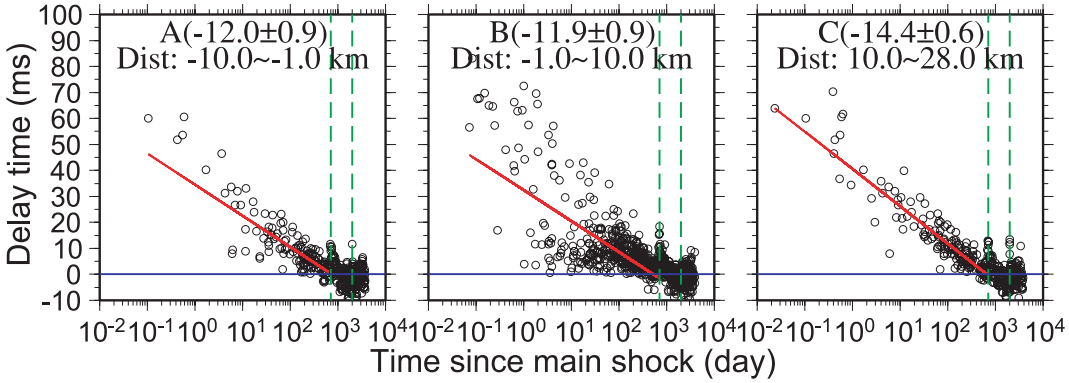

Figure 7. Median delay time plotted against the logarithmic elapsed time after the 1984 Morgan Hill earthquake for the vertical-component seismograms recorded at station CCO from three segments marked in Fig. 1b. The along-strike distance of the corresponding segment is labeled within each panel. Other symbols are the same as Fig. 5.

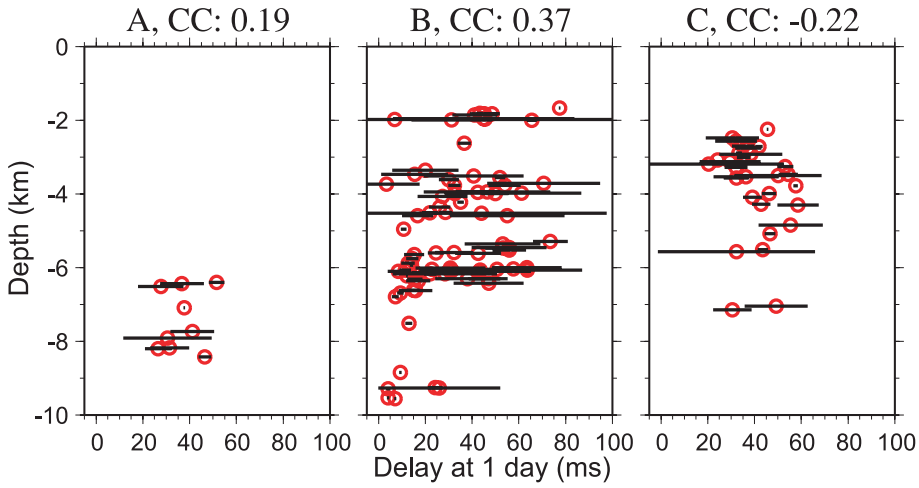

Figure 8. Delay-time at one day after the 1984 main shock versus depths of events recorded at station CCO from different segments (Fig. 1b). Other symbols are the same as Fig. 6.

observed temporal changes. The largest temporal changes are found at station CCO that is the closest to the rupture zone of the Morgan Hill main shock. In addition, the temporal changes are larger in the top 6 km and decrease systematically at larger depth. Due to the close proximity of the CCO station to the rupture zone of the Morgan Hill main shock, we suggest that the observed temporal changes are related to the low-velocity damage zone around the Calaveras fault. In comparison, the temporal changes at the other five stations are much smaller, and do not show clear relationship with hypocentral depth. We infer that the observed temporal changes at these five stations mostly occur in the top few hundred metres of the near-surface layers, consistent with previous results in this region (Rubinstein & Beroza 2004a,b; Schaff & Beroza 2004).

Similar to previous studies (e.g. Rubinstein & Beroza 2004a; Peng & Ben-Zion 2006), we invoke non-linear site response to explain the relatively small temporal changes at the five stations. Laboratory simulations and field observations have shown the reductions of both shear wave velocity and amplification effects in shallow soil layers due to the non-linear elastic behaviour under large shear strains (Beresnev & Wen 1996; Johnson *et al.* 1996; Sawazaki *et al.* 2006). In this situation, considerable seismic energy is consumed to create new fractures and open existing cracks, which in turn effectively reduce the seismic velocity (Rubinstein & Beroza 2004a; Schaff & Beroza 2004; Peng & Ben-Zion 2006), and increase attenuation (Chun *et al.* 2004) during strong ground motions. Because the non-linearity is generally prohibited with increasing confining pressure, the coseismic damage and temporal changes are likely constrained at shallow depth, consistent with the observed patterns (Figs 5 and 6) for these five stations. The interpolated time delay 15 min (0.25 hr) after the main shock is about 5–10 ms. If we assume that the damage zone is confined in the top 200 m of the shallow layer with an average *S*-wave velocity of 1.0 km s^{-1}, the estimated minimum coseismic *S*-wave velocity drop near these five stations is about 2.5–5 per cent, which is compatible with the observation of Schaff & Beroza (2004) in the same region.

In comparison, the temporal changes observed at station CCO are much larger and show weak dependence with hypocentral depth. The rock unit at station CCO is Knoxville Formation (Rubinstein & Beroza 2004a), which is the lowest part of the Great Valley Sequence deposited during late Jurassic to early Cretaceous. It is mainly dark, greenish and grey shale with sandstone interbeds and could locally include conglomeratic sandstone in the lower part (Graymer *et al.* 1994). Phillips & Aki (1986) studied the local site amplification in central California using the decay of coda waves, and found that stations with large positive site amplification factor also observed strong velocity changes after the 1979 Coyote Creek earthquake immediately south of our study region (Poupinet *et al.* 1984). This is consistent with the aforementioned explanation that the velocity

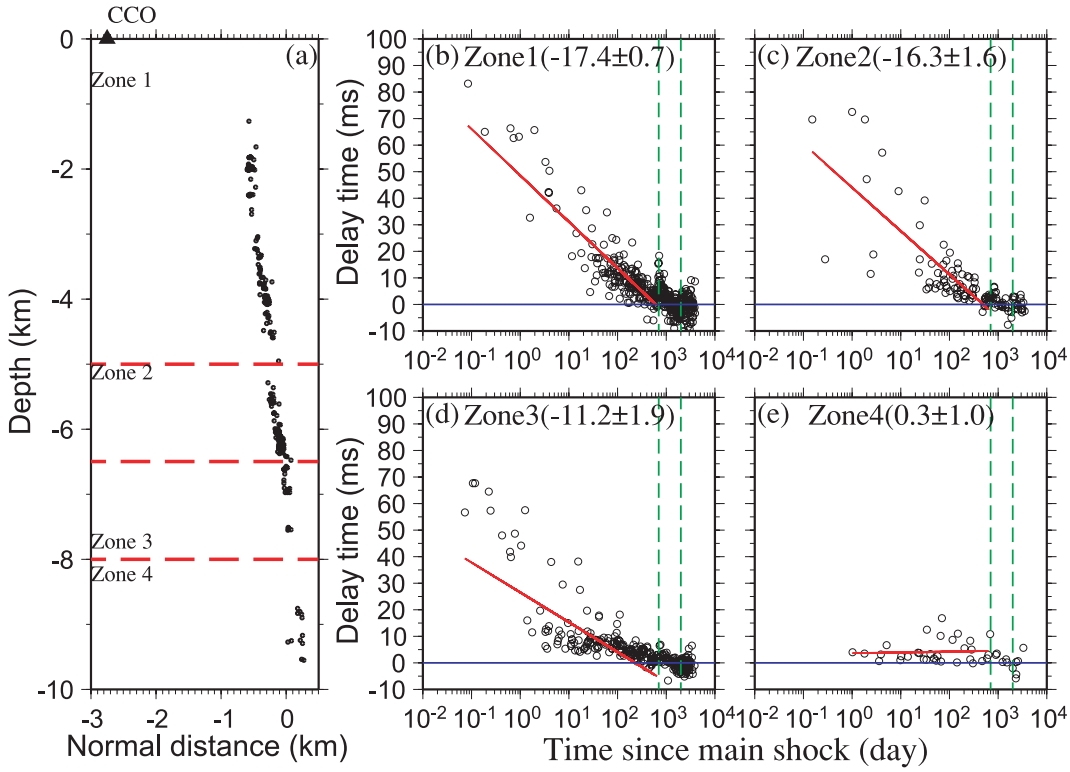

Figure 9. (a) Cross-section views of seismicity in Segment B perpendicular to the strike of the fault. The along-strike distance of these seismicity are from −1 to 10 km. The seismicity is further divided into four zones based on the depths range (red dashed lines). (b)–(e) Median delay time for the S coda waves plotted against the logarithmic elapsed time after the 1984 Morgan Hill earthquake for the vertical-component seismograms recorded at station CCO from different segments (Fig. 9a). Other symbols are the same as Fig. 5.

changes for most stations are caused by temporal changes in local site effects. Rubinstein & Beroza (2004a) also used the correlations between the coda amplification factors and the observed temporal changes to argue for the existence of widespread non-linear strong ground motion. We note, however, that the coda amplification factor for CCO is only about −0.9 (Phillips & Aki 1986; Rubinstein & Beroza 2004a), which is not expected to generate large seismic velocity drop near this station. In summary, we suggest that temporal changes observed at station CCO are likely accumulating at larger depth, rather than in the near-surface layer alone.

The synthetic calculation in Appendix A showed that for a station inside a FZ with uniform thickness and coseismic reduction of FZ velocities, the observed median time delay increases systematically with increasing depth, while the slope of the time delay remains near constant. To explain the decrease of time delay with increasing depth at station CCO, we need to place most of the sampled temporal changes in the top few kilometres of the FZ. A common FZ structure as inferred from previous seismic refraction measurements and 3-D tomographic studies is a wedge-shape model that is wider in the top few kilometres and narrower at larger depth (e.g. Cormier & Spudich, 1984; Blümling *et al.* 1985; Mooney & Colburn 1985; Mooney & Ginzburg 1986; Michael 1988). Such a wedge-shape FZ model is also consistent with a hierarchical flower structure as inferred from recent observations of FZ trapped waves (e.g. Rovelli *et al.* 2002; Ben-Zion *et al.* 2003; Peng *et al.* 2003; Lewis *et al.* 2005; Cochran *et al.* 2009), near-fault crustal anisotropy (Cochran *et al.* 2003, 2006; Peng & Ben-Zion 2004; Zhang *et al.* 2007), and geological studies of strike-slip FZs (e.g. Sylvester 1988; Rockwell & Ben-Zion 2007). Here, we attempt to use such wedge-shape FZ model to explain the observed temporal changes in this study.

The Calaveras fault, like many other active plate-boundary faults (e.g. Ben-Zion & Sammis 2003), is characterized by localized belts of damage zones that have considerably lower elastic moduli than the surrounding rocks (Mooney & Colburn 1985; Spudich & Olsen 2001). The inferred low-velocity FZ in this region has a width of about 1–2 km at surface (Blümling *et al.* 1985), and extends to the depth of approximately 5 km (Michael 1988). Such low-velocity FZ is likely a cumulative effect due to faulting related damages during major earthquakes such as the 1984 Morgan Hill main shock, and probably long-term creeps localized in the shallow crust (Templeton *et al.* 2009). Cormier & Spudich (1984) computed synthetic seismograms based on a wedge-shaped low-velocity zone around the Calaveras fault, and found clear focusing of seismic ray within the wedge, consistent with the observations of local amplification within the FZ in previous studies.

Station CCO is about 80 m to a mapped Holocene-active fault at surface (measured from USGS Quaternary-active fault map of San Francisco Bay area), and is about 2 km from the main strand of the Calaveras fault interface as inferred from the surface projection of the active seismicity (Figs 1 and 9). Clear FZ head waves (Zhao & Peng 2008) and possible signals of FZ trapped waves (e.g. Fig. 4) are observed at station CCO, indicating that this station is very close to the Calaveras FZ. We suggest that the observed temporal changes at station CCO are mostly confined in the wedge-shaped low-velocity zone as inferred from previous seismic refraction measurements (Blümling *et al.* 1985; Mooney & Colburn 1985) and 3-D tomographic studies (Michael 1988). Because of the intrinsic weakness,

its close distance to the dynamic rupture of the 1984 Morgan Hill main shock, and the focusing effects within the wedge, the Calaveras FZ beneath CCO probably experience strong shaking and large dynamic stresses during the main shock, resulting in further damages in material strength and subsequent recoveries. In addition, because the wedge-shaped damage zone is most prominent at shallow depth, seismic rays from repeating earthquakes in the top few kilometres of the fault provide an adequate sampling of the damage zone, resulting in large time delays. In comparison, seismic rays for deeper clusters could have a significant portion sampling the less-damaged host rock before reaching the station CCO. Hence, the observed time delays are much smaller than those at shallower depth.

In this study, we found that the inferred damage zone around CCO is most prominent in the top 5–6 km, and the degrees of damage decrease systematically at larger depth. Hence, the observed temporal changes are largely accumulating above the main shock rupture patches at the depth range of 6–8 km beneath station CCO, as obtained from kinematic slip inversions (Beroza & Spudich 1988). Previous studies have suggested that the propagating crack tip of an earthquake rupture could induce large dynamic stress and generate significant damages around the ruptured FZ (Li *et al.* 2006; Ma 2008). However, our results inferred a rather small temporal change around the ruptured region at depth (e.g. Fig. 9).

A potential bias of small temporal changes at larger depth (e.g. 8–10 km) is the lack of repeating earthquakes in this depth range, especially in the first few hours immediately after the main shock, and a few years afterwards (e.g. Fig. 9). The lack of early repeating aftershocks could be explained by a delayed response of post-seismic creep at larger depth (e.g. Peng & Zhao 2009), while the lack of late repeating aftershocks is likely due to the diminishing strain rate and post-seismic shallowing of the brittle–ductile transition zone at depth (e.g. Schaff *et al.* 2002; Rolandone *et al.* 2004; Kaneko & Lapusta, 2008). To rule out such bias, we have chosen to extrapolate the time delays to 1 d after the main shock so that there are enough data points at larger depth to provide constraints. While the lack of late repeating aftershocks may lower the coseismic changes, such effect is minor because the majority of the coseismic change is recovered in the first few months due to the logarithmic dependence of time. However, if permanent damages occurred coseismically (e.g. Schaff & Beroza 2004), the extrapolated 1-d time delays would be lower bound estimate of the true coseismic changes. In addition, we only fit the data before the occurrence of the Mt Lewis earthquake in 1986 March 31, when the majority of the deep cluster ends. Hence, we argue that the observed depth-dependent effects are unlikely to be purely caused by less sampling points at larger depth, but rather represent a genuine feature of damage suppression with increasing depth.

An alternative explanation is that large coseismic changes do occur below 6 km, due to the close proximity of the rupture zone at 6–8 km. However, the temporal changes are not sampled adequately by the deep clusters for the following reasons. First, as mention before, the seismic rays from the deep clusters could leave the deep FZ that is highly damaged, propagate mainly in the less damaged host rocks, and finally bend towards the FZ to be recorded at station CCO. In addition, if the damage zone is so highly localized at seismogenic depth (e.g. Ma 2008) that the width of the damage zone is much smaller than the wavelength of the seismic waves, such localized damages may not be detected (Wu *et al.* 2008). Another possibility is that the coseismic damages at 6 km and larger depth recover faster in the first few hours because of the higher confining pressure at larger depth (Finzi *et al.* 2009), leaving small temporal changes to be observed at later times. Unfortunately, our repeating cluster is derived from the relocated catalogue of Schaff *et al.* (2002) with many early aftershocks (and presumably repeating aftershocks) missing in the first few hours after the main shock (Peng *et al.* 2006, 2007). Hence, at present we do not have enough temporal resolutions to favour or rule out such possibility. A systematic search of missing repeating aftershocks immediately after the main shock (e.g. Lengliné & Marsan 2009; Peng & Zhao 2009) may help to provide important constraints on whether large coseismic changes and fast post-seismic recovery occur at larger depth or not.

In addition to the distances to and depth within the active FZ, the rupture direction of the 1984 main shock could also play an important role in controlling the observed temporal changes. It is well known that radiated seismic energy is concentrated in the rupture direction due to the so-called directivity effect. Because the rupture direction of the 1984 Morgan Hill earthquake is to the SE (Bakun *et al.* 1984), we expect larger ground motions and hence larger temporal changes for station in that direction. For example, stations CAL, CSC, and CMH are all close to active FZs, but the observed temporal changes are not as large as that of CCO, which could be due to the fact that these stations were not in the rupture direction of the Morgan Hill main shock, and hence experienced relatively small strong ground motions. Station CAD is in the rupture direction, but is relatively far from the Calaveras fault as compared with station CCO. Overall, our observations are consistent with the previous inferences that the stations with large temporal changes are generally close to the rupture zone of the main shock, and have experienced large coseismic strong ground motions (Rubinstein & Beroza 2004a,b; Rubinstein *et al.* 2007; Schaff & Beroza 2004; Peng & Ben-Zion 2006).

As mentioned before, recent 3-D dynamic rupture simulations have produced widespread inelastic strains in the near-surface layers and localized flower-like inelastic zones around active FZs at depth (Ma 2008; Finzi *et al.* 2009). The flower-type structure is a direct result of damage suppression due to increasing confining pressure with depth. Ma (2008) also suggested that widespread near-surface inelastic strains are mainly caused by strong seismic waves, and the narrow inelastic zone at depth is mainly induced by dynamic stresses associated with the rupture front. Another recent study based on InSAR images has shown a clear subsidence of the surface after the 2003 Bam earthquake in Iran (Fielding *et al.* 2009). They suggested that post-seismic subsidence/compaction is likely associated with the healing processes in the shallow FZ that is coseismically damaged during the main shock. In this study, we found that the temporal changes at the other five stations away from the Calaveras fault that ruptured during the Morgan Hill earthquake are mainly constrained in the near-surface layers, while at station CCO we attributed the observed temporal changes to the damage zone associated with the Calaveras fault at larger depth. Hence, our observations are generally consistent with these recent numerical simulations (Ma 2008; Finzi *et al.* 2009) and geodetic observations (Fielding *et al.* 2009).

We note that the coseismic damages and recovery processes observed in this study are associated with a single main shock. Over the geological time scales, such repeated damages and healing processes may produce permanent changes inside active faults, and hence could play an important role in the evolutions of the FZ structures (e.g. Ben-Zion & Sammis 2003; Ma 2008; Cochran *et al.* 2009; Finzi *et al.* 2009) and near-surface layers. Such permanent change, however, may be a very subtle signal for one or a few main shocks. Repeating earthquakes throughout the earthquake cycle (or

at least before and after the main shock) are needed to detect such changes (e.g. Schaff and Beroza 2004).

In summary, our observations are consistent with the widespread damages in the top few hundred metres of the shallow crust (Rubinstein & Beroza 2004a, 2005; Peng & Ben-Zion 2006), and localized temporal changes in and around active FZs at seismogenic depths (Schaff & Beroza 2004; Li *et al.* 2006; Rubinstein *et al.* 2007; Taira *et al.* 2008). These results also support the numerical simulations of widespread damages in the near surface and localized damages around active FZs at depth (Ma 2008; Finzi *et al.* 2009). Recent studies have also shown that shaking induced damages may offer an explanation for dynamic triggering of earthquakes (Johnson & Jia 2005), and generations of high-frequency extreme ground motions in the near surface layers (Fischer *et al.* 2008; Sleep & Ma 2008). Hence, systematic observations of temporal changes from repeating earthquakes not only provide additional evidence of widespread non-linearity during strong ground motions, but also offer new insight into the long-term evolutions of FZ structures and interactions of earthquakes and faults.

ACKNOWLEDGMENTS

The data are downloaded from Northern California Earthquake Data Center (NCEDC). The Quaternary-active fault map and the detailed geological map of San Francisco Bay area are obtained from USGS webpage. We thank Fenglin Niu for sharing the sliding window cross-correlation code, Yehuda Ben-Zion for sharing the FZ trapped waves synthetic code, and David Schaff for making the Schaff *et al.* (2002) relocated catalogue available on his website. The main shock slip distribution of Beroza & Spudich (1988) is obtained from Martin Mai's SRCMOD online database. The manuscript benefited from valuable comments by Justin Rubinstein, Roland Bürgmann, the reviewers David Schaff and Shuo Ma and the Editor Jeannot Trampert. The study was funded by the National Science Foundation (grant EAR-0710959).

REFERENCES

Aki, K., 1969. Analysis of seismic coda of local earthquakes as scattered waves, *J. geophys. Res.,* **74,** 615–631.

Baisch, S. & Bokelmann, G.H.R., 2001. Seismic waveform attributes before and after the Loma Prieta earthquake: scattering change near the earthquake and temporal recovery, *J. geophys. Res.,* **106**(B8), 16 323–16 337.

Bakun, W.H., Clark, M.M., Cockerham, R.S., Ellsworth, W.L., Lindh, A.G., Prescott, W.H., Shakal, A.F. & Spudich, P., 1984. The 1984 Morgan Hill, California, earthquake, *Science,* **225,** 288–291, doi:10.1126/science.225.4659.288.

Ben-Zion, Y., 1998. Properties of seismic fault zone waves and their utility for imaging low velocity structures, *J. geophys. Res.,* **103,** 12 567–12 585.

Ben-Zion, Y. & Aki, K., 1990. Seismic radiation from an SH line source in a laterally heterogeneous planar fault zone, *Bull. seism. Soc. Am.,* **70,** 971–994.

Ben-Zion, Y. & Sammis, C.G., 2003. Characterization of fault zones, *Pure appl. Geophys.,* **160,** 677–715.

Ben-Zion, Y. *et al.*, 2003. A shallow fault zone structure illuminated by trapped waves in the Karadere-Duzce branch of the north Anatolian fault, western Turkey, *Geophys. J. Int.,* **152,** 699–717, doi:10.1046/j.1365-246X.2003.01870.x.

Beresnev, I.A. & Wen, K.-L., 1996. Nonlinear soil response—a reality? *Bull. seism. Soc. Am.,* **86,** 1964–1978.

Beroza, G.C. & Spudich, P., 1988. Linearized inversion for fault rupture behavior: application to the 1984, Morgan Hill, California, earthquake, *J. geophys. Res.,* **93,** 6275–6296.

Blümling, P., Mooney, W.D. & Lee, W.H.K., 1985. Crustal structure of the southern Calaveras fault zone, central California, from seismic refraction investigations, *Bull. seism. Soc. Am.,* **75**(1), 193–209.

Brenguier, F., Shapiro, N.M., Campillo, M., Ferrazzini, V., Duputel, Z., Coutant, O. & Nercessian, A., 2008a. Towards forecasting volcanic eruptions using seismic noise, *Nat. Geosci.,* **1,** doi:10.1038/ngeo104.

Brenguier, F., Campillo, M., Hadziioannou, C., Shapiro, N.M., Nadeau, R.M. & Larose, E., 2008b. Postseismic relaxation along the San Andreas Fault at Parkfield from continuous seismological observations, *Science,* **321,** 1478–1481.

Chao, K., & Peng, Z. 2009. Temporal changes of seismic velocity and anisotropy in the shallow crust induced by the 1999 October 22 *M*6.4 Chia-Yi, Taiwan earthquake, *Geophys. J. Int.,* doi:10.1111/j.1365-246X.2009.04384.x (this issue).

Chun, K.-Y., Henderson, G.A. & Liu, J., 2004. Temporal changes in *P* wave attenuation in the Loma Prieta rupture zone, *J. geophys. Res.,* **109,** B02317, doi:10.1029/2003JB002498.1029/2003JB002498.

Cochran, E.S., Vidale, J.E. & Li, Y.-G., 2003. Near-fault anisotropy following the Hector Mine earthquake, *J. geophys. Res.,* **108**(B9), 2436, doi:10.1029/2002JB002352.

Cochran, E.S., Li, Y.-G. & Vidale, J.E., 2006. Anisotropy in the shallow crust observed around the San Andreas Fault before and after the 2004 M6 Parkfield earthquake, *Bull. seism. Soc. Am.,* **96,** S364–S375.

Cochran, E.S., Li, Y.-G., Shearer, P.M., Barbot, S., Fialko, Y. & Vidale, J.E., 2009. Seismic and geodetic evidence for extensive, long-lived fault damage zones, *Geology,* **37,** 315–318, doi:10.1130/G25306A.1.

Cormier, V.F. & Spudich, P., 1984. Amplification of ground motion and waveform complexities in fault zones: examples from the San Andreas and the Calaveras faults, *Geophys. J. R. astr. Soc.,* **79,** 135–152.

Eshelby, J.D., 1957. The determination of the elastic field of an ellipsoidal inclusion and related problems, *Proc. R. Soc. Lond., Ser. A,* **241,** 76–396.

Fielding, E.J., Lundgren, P.R., Bürgmann, R. & Funning, G.J., 2009. Shallow fault-zone dilatancy recovery after the 2003 Bam earthquake in Iran, *Nature,* **458,** doi:10.1038/nature07817.

Finzi, Y., Hearn, E.H., Ben-Zion, Y. & Lyakhovsky, V., 2009. Structural properties and deformation patterns of evolving strike-slip faults: numerical simulations incorporating damage rheology, *Pure appl. Geophys.,* **166,** 1537–1573, doi:10.1007/s00024-009-0522-1.

Fischer, A.D., Peng, Z. & Sammis, C.G., 2008. Dynamic triggering of high-frequency bursts by strong motions during the 2004 Parkfield earthquake sequence, *Geophys. Res. Lett.,* **35,** L12305, doi:10.1029/2008GL033905.

Graymer, R.W., Jones, D.L. & Brabb, E.E., 1994. Preliminary geologic map emphasizing bedrock formations in Contra Costa County, California: a digital database, *U.S. Geol. Surv. Open-File Rept.* 94–622.

Haney, M.M., van Wijk, K., Preston, L.A. & Aldridge, D.F., 2009. Observation and modeling of source effects in coda wave interferometry at Pavlof volcano, *Leading Edge,* **28,** 554–560, doi:10.1190/1.3124930.

Johnson, P.A. & Jia, X., 2005. Nonlinear dynamics, granular media and dynamic earthquake triggering, *Nature,* **437,** 871–874, doi:10.1038/nature04015.

Johnson, P.A., Zinszner, B. & Rasolofosaon, P.N.J., 1996. Resonance and elastic nonlinear phenomena in rock, *J. geophys. Res.,* **101**(B5), 11 553–11 564.

Karabulut, H. & Bouchon, M., 2007. Spatial variability and non-linearity of strong ground motion near a fault, *Geophys. J. Int.,* **170,** 262–274, doi:10.1111/j.1365-246X.2007.03406.x.

Kaneko, Y. & Lapusta, N., 2008. Variability of earthquake nucleation in continuum models of rate-and-state faults and implications for aftershock rates, *J. geophys. Res.,* **113,** B12312, doi:10.1029/2007JB005154.

Lengliné, O. & Marsan, D., 2009. Inferring the coseismic and postseismic stress changes caused by the 2004, Mw = 6 Parkfield earthquake from variations of recurrence times of microearthquakes, *J. geophys. Res.,* **114,** B10303, doi:10.1029/2008JB006118.

Lewis, M.A., Peng, Z., Ben-Zion, Y. & Vernon, F.L., 2005. Shallow seismic trapping structure in the San Jacinto fault zone near Anza, California, *Geophys. J. Int.,* **162**(3), 867–881, doi:10.1111/j.1365-246X.2005.02684.

Li, Y.-G., Chen, P., Cochran, E.S., Vidale, J.E. & Burdette, T., 2006. Seismic evidence for rock damage and healing on the San Andreas fault associated

with the 2004 M 6.0 Parkfield earthquake, *Bull. seism. Soc. Am.,* **96**(4B), 349–363.

Ma, S., 2008. A physical model for widespread near-surface and fault zone damage induced by earthquakes, *Geochem. Geophys. Geosyst.,* **9,** Q11009, doi:10.1029/2008GC002231.

Manaker, D.M., Michael, A.J. & Bürgmann, R., 2005. Subsurface structure and kinematics of the Calaveras-Hayward fault stepover from three-dimensional Vp and seismicity, San Francisco Bay Region, California, *Bull. seism. Soc. Am.,* **95**(2), 446–470.

Menke, W., 1999. Using waveform similarity to constrain earthquake locations, *Bull. seism. Soc. Am.,* **89,** 1143–1146.

Michael, A., 1988. Effects of three-dimensional velocity structure on the seismicity of the 1984 Morgan Hill, California, aftershock sequence, *Bull. seism. Soc. Am.,* **78,** 1199–1221.

Mooney, W.D. & Colburn, R.H., 1985. A seismic-refraction profile across the San Andreas, Sargent, and Calaveras faults, west-central California, *Bull. seism. Soc. Am.,* **75,** 175–191.

Mooney, W.D. & Ginzburg, A., 1986. Seismic measurements of the internal properties of fault zones, *Pure appl. Geophys.,* **124,** 141–157.

Nadeau, R.M., Foxall, W. & McEvilly, T.V., 1995. Clustering and periodic recurrence of microearthquakes on the San Andreas Fault at Parkfield, California, *Science,* **267,** 503–507.

Nishimura, T. *et al*., 2005. Temporal changes in seismic velocity of the crust around Iwate volcano, Japan, as inferred from analyses of repeated active seismic experiment data from 1998 to 2003, *Earth Planets Space,* **57,** 491–505.

Niu, F., Silver, P.G., Nadeau, R.M. & McEvilly, T.V., 2003. Stress-induced migration of seismic scatters associated with 1993 Parkfield aseismic transient event, *Nature,* **426,** 544–548.

Ohmi, S., Hirahara, K., Wada, H. & Ito, K., 2008. Temporal variations of crustal structure in the source region of the 2007 Noto Hanto Earthquake, central Japan, with passive image interferometry, *Earth Planets Space,* **60**(10), 1069–1074.

Oppenheimer, D.H., Bakun, W.H. & Lindh, A.G., 1990. Slip partitioning of the Calaveras fault, California, and prospects for future earthquakes, *J. geophys. Res.,* **95,** 8483–8498.

Peng, Z. & Ben-Zion, Y., 2004. Systematic analysis of crustal anisotropy along the Karadere-Duzce branch of the north Anatolian fault, *Geophys. J. Int.,* **159,** 253–274, doi:10.1111/j.1365–246X.2004.02379.x.

Peng, Z. & Ben-Zion, Y., 2005. Spatio-temporal variations of crustal anisotropy from similar events in aftershocks of the 1999 M7.4 İzmit and M7.1 Duzce, Turkey, earthquake sequences, *Geophys. J. Int.,* **160,** 1027–1043, doi:10.1111/j.1365-246X.2004.02379.x.

Peng, Z. & Ben-Zion, Y., 2006. Temporal changes of shallow seismic velocity around the Karadere-Duzce branch of the North Anatolian fault and strong ground motion, *Pure appl. Geophys.,* **163,** 567–599.

Peng, Z. & Zhao, P., 2009. Migration of the Parkfield early aftershock sequence, *Nat. Geosci.,* submitted.

Peng, Z., Ben-Zion, Y., Michael, A.J. & Zhu, L., 2003. Quantitative analysis of fault zone waves in the rupture zone of the Landers, 1992, California earthquake: evidence for a shallow trapping structure, *Geophys. J. Int.,* **155,** 1021–1041, doi:10.1111/j.1365-246X.2003.02109.x

Peng, Z., Vidale, J.E., Marone, C. & Rubin, A., 2005. Systematic variations in recurrence interval and moment of repeating aftershocks, *Geophys. Res. Lett.,* **32**(15), L15301, doi:10.1029/2005GL022626.

Peng, Z., Vidale, J.E. & Houston, H., 2006. Anomalous early aftershock decay rates of the 2004 M6 Parkfield earthquake, *Geophys. Res. Lett.,* **33,** L17307, doi:10.1029/2006GL026744.

Peng, Z., Vidale, J.E., Ishii, M. & Helmstetter, A., 2007. Seismicity rate immediately before and after main shock rupture from high-frequency waveforms in Japan, *J. geophys. Res.,* **112,** B03306, doi:10.1029/2006JB004386.

Phillips, W.S. & Aki, K., 1986. Site amplification of coda waves from local earthquakes in Central California, *Bull. seism. Soc. Am.,* **76,** 627–648.

Poupinet, G., Ellsworth, W.L. & Frechet, J., 1984. Monitoring velocity variations in the crust using earthquake doublets: an application to the Calaveras fault, California, *J. geophys. Res.,* **89**(B7), 5719–5731.

Rolandone, F., Burgmann, R. & Nadeau, R.M., 2004. The evolution of the seismic-aseismic transition during the earthquake cycle: constraints from the time-dependent depth distribution of aftershocks, *Geophys. Res. Lett.,* **31,** L23610, doi:10.1029/2004GL021379.

Rockwell, T.K. & Ben-Zion, Y., 2007. High localization of primary slip zones in large earthquakes from paleoseismic trenches: observations and implications for earthquake physics, *J. geophys. Res.,* **112,** B10304, doi:10.1029/2006JB004764.

Rovelli, A., Caserta, A., Marra, F. & Ruggiero, V., 2002. Can seismic waves be trapped inside an inactive fault zone? The case study of Nocera Umbra, central Italy, *Bull. seism. Soc. Am.,* **92,** 2217–2232.

Rubin, A.M., 2002. Using repeating earthquakes to correct high-precision earthquake catalogs for time-dependent station delays, *Bull. seism. Soc. Am.,* **92,** 1647–1659.

Rubinstein, J.L. & Beroza, G.C., 2004a. Evidence for widespread nonlinear strong ground motion in the Mw 6.9 Loma Prieta earthquake, *Bull. seism. Soc. Am.,* **94,** 1595–1608.

Rubinstein, J.L. & Beroza, G.C., 2004b. Nonlinear strong ground motion in the M_L 5.4 Chittenden earthquake: evidence that preexisting damage increases susceptibility to further damage, *Geophys. Res. Lett.,* **31,** L23614, doi:10.1029/2004GL021357.

Rubinstein, J.L. & Beroza, G.C., 2005. Depth constraints on nonlinear strong ground motion from the 2004 Parkfield earthquake, *Geophys. Res. Lett.,* **32,** L14313, doi:10.1029/2005GL023189.

Rubinstein, J.L., Uchida, N. & Beroza, G.C., 2007. Seismic velocity reductions caused by the 2003 Tokachi-Oki earthquake, *J. geophys. Res.,* **112,** B05315, doi:10.1029/2006JB004440.

Sawazaki, K., Sato, H., Nakahara, H. & Nishimura, T., 2006. Temporal change in site response caused by earthquake strong motion as revealed from coda spectral ratio measurement, *Geophys. Res. Lett.,* **33,** L21303, doi:10.1029/2006GL027938.

Sawazaki, K., Sato, H., Nakahara, H. & Nishimura, T., 2009. Time-lapse changes of seismic velocity in the shallow ground caused by strong ground motion shock of the 2000 Western-Tottori earthquake, Japan, as revealed from coda deconvolution analysis, *Bull. seism. Soc. Am.,* **99,** 352–366.

Schaff, D.P. & Beroza, G.C., 2004. Coseismic and postseismic velocity changes measured by repeating earthquakes, *J. geophys. Res.,* **109,** B10302, doi:10.1029/2004JB003011.

Schaff, D.P., Bokelmann, G.H.R., Beroza, G.C., Waldhauser, F. & Ellsworth, W.L., 2002. High-resolution image of Calaveras Fault seismicity, *J. geophys. Res.,* **107**(B9), 2186, doi:10.1029/2001JB000633.

Sleep, N.H., 2009. Depth of rock damage from strong seismic ground motions near the 2004 Parkfield mainshock, *Bull. Seismol. Soc. Am.,* **99**(5), 3067–3076, doi:10.1785/0120090065.

Sleep, N.H. & Ma, S., 2008. Production of brief extreme ground acceleration pulses by nonlinear mechanisms in the shallow subsurface, *Geochem. Geophys. Geosyst.,* **9,** Q03008, doi:10.1029/2007GC001863.

Spudich, P. & Olsen, K.B., 2001. Fault zone amplified waves as a possible seismic hazard along the Calaveras fault in central California, *Geophys. Res. Lett.,* **28,** 2533–2536.

Sylvester, A.G., 1988. Strike-slip faults, *Geol. Soc. Am.,* **100,** 1666–1703.

Taira, T., Silver, P.G., Niu, F. & Nadeau, R.M., 2008. Detecting seismogenic stress evolution and constraining fault zone rheology in the San Andreas Fault following the 2004 Parkfield earthquake, *J. geophys. Res.,* **113,** B03303, doi:10.1029/2007JB005151.

Taira, T., Silver, P.G., Niu, F. & Nadeau, R.M., 2009. Seismic evidence for remote triggering of fault-strength changes on the San Andreas fault at Parkfield, *Nature,* **461,** 636–640.

Templeton, D.C., Nadeau, R.M. & Bürgmann, R., 2008. Behavior of repeating earthquake sequences in Central California and the implications for subsurface fault creep, *Bull. seism. Soc. Am.,* **98,** 52–65.

Templeton, D.C., Nadeau, R.M. & Bürgmann, R., 2009. Distribution of postseismic slip on the Calaveras fault, California, following the 1984 M6.2 Morgan Hill earthquake, *Earth planet. Sci. Lett.,* **277,** doi:10.1016/j.epsl.2008.1009.1024.

Vidale, J.E. & Li, Y., 2003. Damage to the shallow Landers fault from the nearby Hector Mine earthquake, *Nature,* **421,** 524–426.

Waldhauser, F. & Ellsworth, W.L., 2000. A double-difference earthquake location algorithm: method and application to the northern Hayward Fault, *Bull. seism. Soc. Am.,* **90,** 1330–1368.
Waldhauser, F. & Ellsworth, W.L., 2002. Fault structure and mechanics of the Hayward Fault, California, from double-difference earthquake locations, *J. geophys. Res.,* **107**(B3), 2054, doi:10.1029/2000JB000084.
Waldhauser, F. & Schaff, D.P., 2008. Large-scale relocation of two decades of Northern California seismicity using cross-correlation and double-difference methods, *J. geophys. Res.,* **113,** B08311, doi:10.1029/2007JB005479.
Waldhauser, F., Ellsworth, W.L., Schaff, D.P. & Cole, A., 2004. Streaks, multiplets, and holes: high-resolution spatio-temporal behavior of Parkfield seismicity, *Geophys. Res. Lett.,* **31,** L18608, doi:10.1029/2004GL020649.
Wegler, U. & Sens-Schönfelder, C., 2007. Fault zone monitoring with passive image interferometry, *Geophys. J. Int.,* **168,** 1029–1033.
Wegler, U., Nakahara, H., Korn, M. & Shiomi, K., 2009. Sudden drop of seismic velocity after the 2004 Mw 6.6 Mid-Niigata earthquake, Japan, observed with passive image interferometry, *J. geophys. Res.,* **114,** B06305, doi:10.1029/2008JB005869.
Wu, J., Hole, J.A., Snoke, J.A. & Imhof, M.G., 2008. Depth extent of the fault zone seismic waveguide: effects of increasing velocity with depth, *Geophys. J. Int.,* **173,** 611–622.
Wu, C., Peng, Z. & Ben-Zion, Y., 2009a. Non-linearity and temporal changes of fault zone site response associated with strong ground motion, *Geophys. J. Int.,* **176,** 265–278, doi:10.1111/j.1365-246X.2008.04005.x.
Wu, C., Peng, Z. & Assimaki, D., 2009b. Temporal changes of site response associated with strong ground motion of 2004 Mw6.6 Niigata earthquake sequences in Japan, *Bull. seism. Soc. Am.,* doi:10.1785/0120090108.
Xu, Z.J. & Song, X., 2009. Temporal changes of surface wave velocity associated with major Sumatra earthquakes from ambient noise correlation, *Proc. Natl. Acad. Sci. USA,* **106**(34), 14 207–14 212.
Zhang, H., Liu, Y., Thurber, C. & Roecker, S., 2007. Three-dimensional shear-wave splitting tomography in the Parkfield, California, region, *Geophys. Res. Lett.,* **34,** L24308, doi:10.1029/2007GL031951.
Zhao, P. & Peng, Z., 2008. Velocity contrast along the Calaveras fault from analysis of fault zone head waves generated by repeating earthquakes, *Geophys. Res. Lett.,* **35,** L01303, doi:10.1029/2007GL031810.
Zhou, Y., McNally, K.C. & Lay, T., 1993. Analysis of the 1986 Mt. Lewis, California, earthquake: preshocks sequence-main shock-aftershock sequence, *Phys. Earth planet. Inter.,* **75,** 267–288.
Zinszner, B., Johnson, P.A. & Rasolofosaon, P.N.J., 1997. Influence of change in physical state on elastic nonlinear response in rock: significance of effective pressure and water saturation, *J. geophys. Res.,* **102**(B4), 8105–8120.

APPENDIX A

To evaluate the ability of inferring the depth extent of the damage zone, we measure temporal changes from synthetic seismograms generated by SH-type dislocations at different depths inside a low-velocity FZ layer (Fig. A1) sandwiched between a half-space (HS). We use the 2-D analytical solution of Ben-Zion & Aki (1990) and Ben-Zion (1998) to calculate the synthetic waveforms. The initial FZ model parameters are: FZ width $W = 100$ m, S-wave velocities in the FZ and the HS $\beta_{\rm FZ} = 1.5$ km s^{-1} and $\beta_{\rm HS} = 3.0$ km s^{-1}, and quality factors in the FZ and the HS $Q_{\rm FZ} = 50$ and $Q_{\rm HS} = 1000$. The densities of rocks are set to be 2.7 g cm^{-3} for different layers. The station is placed in the middle of the FZ at the free surface (i.e. 50 m to the left-hand boundary of the FZ). The shear dislocation sources are placed along the left-hand boundary of the FZ from 1 to 10 km at depth with interevent spacing of 1 km (Fig. A1). To simulate the velocity reduction inside the FZ, we change $\beta_{\rm FZ}$ to be 1.4925 km s^{-1} (0.5 per cent reduction) and keep $\beta_{\rm HS} = 3.0$ km s^{-1} to be the same.

We use the same procedure as described in Section 3 to measure temporal changes for events at different depths (Fig. A2), except

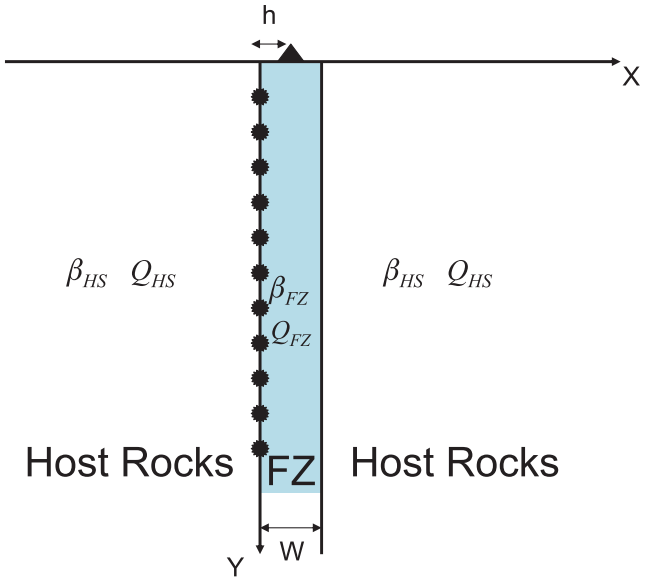

Figure A1. A schematic model showing two quarter spaces separated by a uniform low-velocity FZ structure. The seismic sources are an array of SH line dislocation along the left-hand boundary of the FZ from 1 km to 10 km depth with interevent distance of 1 km. The width, shear wave velocity, and shear attenuation coefficient the FZ are marked by W, β_{FZ} and Q_{FZ}, respectively. The shear wave velocity and the attenuation coefficient of the two quarters spaces are denoted by β_{HS} and Q_{HS}, respectively. The station is located to the right-hand side of the left-hand boundary of the FZ with $h = 50$ m.

slight difference in the following two parameters. First, we first bandpass filtered the seismograms at 1–10 Hz, rather than 1–20 Hz, in order to remove potential high-frequency noise generated by the synthetic code. In addition, we use 0.5-s time window, instead of 1-s window to measure the temporal changes. The primary reason is that the duration of the synthetic FZ trapped waves is less than 1 s for events at depth smaller than 3 km. Hence, a smaller time window is needed to quantify the subtle changes in the time delays.

Fig. A2 shows that the seismograms after reducing the FZ velocity are very similar with the original waveforms at the beginning time, and show gradual increase of delays in the later time. We use a time window starting from the first S arrival to the end of the FZ trapped waves to measure the median value of delay times. We find an clear increase of median delay-times versus depths, which is mainly due to the development of FZ trapped waves with increasing propagation distance, and subsequent increase of time duration of wave trains from those deeper events (e.g. Peng *et al.* 2003). In comparison, the slope measured from the time delays tends to be a constant value for those deeper events. It is interesting to note that most slopes (from events deeper than 2 km) are less than 0.5 per cent and decrease with depths. This is because that the measured slopes reflect a combined effect of velocity reduction within the FZ (0.5 per cent) and the host rocks (0 per cent). As an event occurs deeper, more seismic energy will travel through the host rocks, efficiently deceasing measured velocity reduction (i.e. slope). This observation is similar to those found by Haney *et al.* (2009) for small velocity changes within volcanic conduits. Because the median delay times increase systematically with depth, while the slopes do not, we conclude that median delay-time values provide a better way to infer the relationship between temporal changes and hypocentral depths.

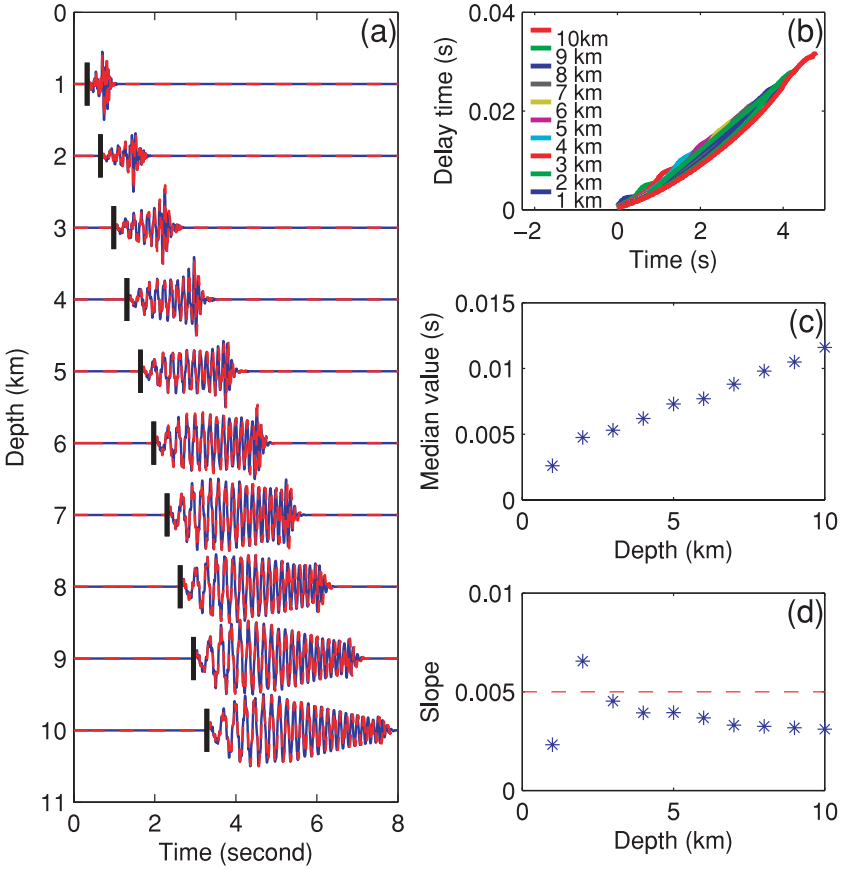

Figure A2. (a) Synthetic waveforms generated at different depths. Original traces and seismograms after velocity-reduction in the FZ are marked by the blue solid lines and red dashed lines, respectively. The first arrivals of *S*-waves arrival are marked by the black vertical lines. (b) Calculated delay-time $\tau(t)$ of events at different depths. All traces are aligned relative to the first arrivals of *S* waves of the corresponding waveforms. (c) Median values of calculated delay-time $\tau(t)$ in (b) versus depths. The median values are calculated from a time-window ranging from the first *S* arrival to the end of FZ trapped waves. (d) The calculated slopes of delay-time $\tau(t)$ in (b) versus depths. The slope is calculated at a 0.7-s time window starting from first *S* arrivals. The horizontal red dashed line marks the input value of 0.5 per cent reduction in FZ velocities.